

OPEN ACCESS

Repository of the Max Delbrück Center for Molecular Medicine (MDC) in the Helmholtz Association

<http://edoc.mdc-berlin.de/11010>

Neuron-astrocyte interactions in the medial nucleus of the trapezoid body

Reyes-Haro, D. and Mueller, J. and Boresch, M. and Pivneva, T. and Benedetti, B. and Scheller, A. and Nolte, C. and Kettenmann, H.

This is a copy of the final article, which was first published online on 17 May 2010 and in final edited form in:

Journal of General Physiology
2010 JUN 01 ; 135(6): 583-594
doi: [10.1085/jgp.200910354](https://doi.org/10.1085/jgp.200910354)

Publisher: [Rockefeller University Press](#)

© 2010 Reyes-Haro et al. This article is distributed under the terms of an Attribution–Noncommercial–Share Alike–No Mirror Sites license for the first six months after the publication date (see <http://www.rupress.org/terms>).



After six months it is available under a Creative Commons License (Attribution–Noncommercial–Share Alike 3.0 Unported license, as described at <http://creativecommons.org/licenses/by-nc-sa/3.0/>).

Neuron–astrocyte interactions in the medial nucleus of the trapezoid body

Daniel Reyes-Haro,^{1,4} Jochen Müller,^{1,5} Margarethe Boresch,¹ Tatjyana Pivneva,² Bruno Benedetti,¹ Anja Scheller,³ Christiane Nolte,¹ and Helmut Kettenmann¹

¹Cellular Neuroscience, Max Delbrück Center for Molecular Medicine, 13092 Berlin, Germany

²Bogomoletz Institute of Physiology, 01024 Kiev, Ukraine

³Max-Planck-Institut für Experimentelle Medizin, 37075 Göttingen, Germany

⁴Departamento de Neurobiología Molecular y Celular, Instituto de Neurobiología, Universidad Nacional Autónoma de México, Campus Juriquilla, Juriquilla, Querétaro 76230, México

⁵Institut für Experimentelle Neurologie, Charité – Universitätsmedizin Berlin, 10117 Berlin, Germany

The calyx of Held (CoH) synapse serves as a model system to analyze basic mechanisms of synaptic transmission. Astrocyte processes are part of the synaptic structure and contact both pre- and postsynaptic membranes. In the medial nucleus of the trapezoid body (MNTB), midline stimulation evoked a current response that was not mediated by glutamate receptors or glutamate uptake, despite the fact that astrocytes express functional receptors and transporters. However, astrocytes showed spontaneous Ca^{2+} responses and neuronal slow inward currents (nSICs) were recorded in the postsynaptic principal neurons (PPNs) of the MNTB. These currents were correlated with astrocytic Ca^{2+} activity because dialysis of astrocytes with BAPTA abolished nSICs. Moreover, the frequency of these currents was increased when Ca^{2+} responses in astrocytes were elicited. NMDA antagonists selectively blocked nSICs while D-serine degradation significantly reduced NMDA-mediated currents. In contrast to previous studies in the hippocampus, these NMDA-mediated currents were rarely synchronized.

INTRODUCTION

Cellular communication via vesicular exocytosis of transmitter is known to occur in neurons (Katz and Miledi, 1965; Miledi, 1973). However, there is growing evidence that astrocytes have the capacity to release transmitters such as glutamate, ATP, and D-serine (Panatier et al., 2006; Fellin et al., 2007; Jourdain et al., 2007). Moreover, a bidirectional communication between astrocytes and neurons has been reported in brain regions such as the hippocampus and nucleus accumbens (Angulo et al., 2004; Fellin et al., 2004; D'Ascenzo et al., 2007; Jourdain et al., 2007; Perea and Araque, 2007; Navarrete and Araque, 2008; Shigetomi et al., 2008). Whether this occurs in brain regions like the brainstem remains unknown.

In mammals, the calyx of Held (CoH) synapse has proven to be a valuable model to study basic mechanisms of synaptic function. The CoH is a giant glutamatergic nerve terminal that contacts postsynaptic principal

neurons (PPNs) of the medial nucleus of the trapezoid body (MNTB) in the auditory pathway. This synapse is specialized for sound localization and requires high frequency signal transmission (for review see von Gersdorff and Borst, 2002; Schneggenburger and Forsythe, 2006). The process involves the globular bushy neurons of the anterior ventral cochlear nucleus that project via their axons to the PPNs of the contralateral MNTB and form an axo-somatic synapse known as the CoH synapse (Kuwabara et al., 1991). Presynaptic activation can be accomplished by electrical stimulation of the axons from the anterior ventral cochlear nucleus or by patch clamping a single CoH terminal (Forsythe, 1994; Barnes-Davies and Forsythe, 1995). This leads to a massive release of glutamate that activates PPNs with large current amplitudes mediated by ionotropic glutamate receptors (Forsythe, 1994; Barnes-Davies and Forsythe, 1995; Joshi and Wang, 2002). Recent morphological studies revealed that glial processes contact the pre- and postsynaptic membranes and express both glutamate receptors and transporters (Elezgarai et al., 2001; Sätzler et al., 2002; Renden et al., 2005). The influence of astrocyte activity on the CoH synapse function has not been

D. Reyes-Haro and J. Müller contributed equally to this paper.

Correspondence to Helmut Kettenmann: kettenmann@mdc-berlin.de

Abbreviations used in this paper: aCSF, artificial cerebrospinal fluid; APV, DL-2-amino-5-phosphonovaleric acid; aSIC, astrocytic slow inward current; BAPTA, 1,2-bis(*o*-aminophenoxy)ethane-*N,N,N',N'*-tetraacetic acid; CNQX, 6-cyano-7-nitroquinoxaline-2,3-dione; CoH, calyx of Held; DAAO, D-amino acid oxidase; D-Asp, D-aspartate; eGFP, enhanced GFP; EPSC, excitatory postsynaptic current; GFAP, glial fibrillary acidic protein; KA, kainic acid; MNTB, medial nucleus of the trapezoid body; mRFP, monomeric RFP; NMDA, *N*-methyl-D-aspartate; nSIC, neuronal slow inward current; PPN, postsynaptic principal neuron; TBOA, threo-β-benzoyloxyaspartate; TTX, tetrodotoxin.

explored. In a recent study we showed that NG2-positive glial cells and PPNs can receive coordinated synaptic input, adding the glial element to synaptic communication at the CoH synapse (Müller et al., 2009). In the present study we demonstrate that astrocytes signal to the PPNs in the MNTB by eliciting slow inward currents.

MATERIALS AND METHODS

Preparation of brain stem slices

All experiments were conducted according to the guidelines of the German Animal Protection Law. For slice preparation, 8–10-d-old outbred NMRI mice (Charles River), transgenic GFAP-mRFP1 mice (Hirrlinger et al., 2005), or transgenic GFAP-eGFP mice (Nolte et al., 2001) were decapitated. Brains were immediately transferred to ice-cold oxygenated artificial cerebrospinal fluid (aCSF) containing (in mM): 134 NaCl, 2.5 KCl, 1.3 MgCl₂, 2 CaCl₂, 1.25 K₂HPO₄, 26 NaHCO₃, and 10 glucose, equilibrated with 95% O₂ and 5% CO₂ to pH 7.4. Transverse brain stem slices (160 µm) were cut using a tissue slicer (Microm HM 650 V; Walldorf). Slices containing the MNTB were stored in gassed aCSF for 30–45 min before experiments. In general, the number of experiments (*n*) refers to the number of neurons recorded. Each recording was made from one slice. For each experimental condition, different slices from different mice were used. The number of experiments is mentioned when (*n*) is used for neuronal slow inward currents (nSICs).

Calcium recording

Dye loading with 10 µM Fluo-4-AM was performed for a 30-min incubation at 37°C. Slices were transferred to the recording chamber of an upright microscope (Axioskop; Carl Zeiss, Inc.) and intracellular Ca²⁺ changes were recorded using a cooled CCD camera (Sensicam; PCO AG) attached to the microscope. The slice was illuminated (490 nm) for 100 ms with a monochromator (Polychrome IV; Till Photonics) and images were acquired every second. Emission was detected with a 510-nm long-pass filter (Chroma Technology Corp.). The monochromator and the CCD camera were controlled and synchronized by TIDA 5.19 software (HEKA). Images were visualized on the PC screen with the Imaging Cells Easily (ICE) software developed in our laboratory operating under the control of TIDA. Images were stored on a PC and processed with conventional software (ImagePro 5.0, Media Cybernetics and Microcal; Origin 7.0, Origin Laboratories). Calcium variations recorded in astrocyte somata (defined as regions of interest) were estimated as changes of fluorescence signal over baseline (F/F₀). The peak of the response was used to normalize the acquired values (normalized F/F₀).

Calcium signals were either recorded spontaneously or elicited with electrical stimulation via a conventional glass electrode filled with aCSF. The stimulation pipette had a tip opening of ~20 µm and was placed on top of the slice, gently touching the upper cell layer. The slice was allowed to recover from mechanical stress for ~5 min. A PPN was approached with a patch electrode (see Electrophysiological recordings) and recording was performed for at least 100 s while superfusing with normal aCSF. The slice was then superfused with normal or modified aCSF (1 µM tetrodotoxin [TTX] was added; Mg²⁺ and Ca²⁺ were omitted) for a 100-s preincubation. The prestimulus was another 100 s with normal or modified aCSF. The calcium signal was then triggered by 40 pulses of 100 µA in 4 s (10 Hz) with a stimulation electrode and recording was undertaken for another 100 s (post-stimulus). The number of nSICs elicited during prestimulus and post-stimulus were counted and the probability of occurrence for each experimental condition was calculated.

Electrophysiological recordings

The MNTB was easily recognized using light microscopy due to the size of the PPNs (~20 µm). Astrocytes and PPN somata were visible in standard water immersion optics and could be approached with a patch pipette. Membrane currents were recorded with the patch-clamp technique using the whole-cell recording configuration (Hamill et al., 1981). Current signals were amplified with a triple EPC 10 (HEKA), filtered at 3 kHz, sampled at 10 kHz, recorded by the TIDA software (5.19) and stored on a personal computer. Input membrane resistance (R_m) and membrane decay time constants (τ) were determined from an average of 10 depolarizing (10 mV = ΔU) current pulses (10 ms). The resulting membrane charging curves were fitted to a single exponential: $I_x = a + b * e^{(x/\tau)}$ and τ was obtained. The membrane capacitance was calculated as C_m = τ/R_a , where R_a is the access resistance.

Patch micropipettes with a resistance of 4–5 MΩ (for the neurons) or 6–8 MΩ (for the astrocytes) were pulled from thin-walled borosilicate glass (outer diameter 1.5 mm, inner diameter 0.87 mm; Hilgenberg) using a P2000 laser-based micropipette puller (Sutter Instrument Co.). The micropipette solution used for neuronal recording (solution A) contained (in mM): 97.5 potassium gluconate, 32.5 CsCl, 5 EGTA, 10 Hepes, 1 MgCl₂, 30 TEA, and 3 lidocaine N-ethyl bromide (QX314). For glial recording (solution B), the internal solution contained (in mM): 120 potassium gluconate, 10 KCl, 1 MgCl₂, 10 Hepes, 0.1 EGTA, 0.025 CaCl₂, 1 K₂ATP, 4 glucose, and 0.2 Na₂ GTP. For dialyzing astrocytes with the Ca²⁺ chelator 1,2-bis(*o*-aminophenoxy)ethane-N,N,N',N'-tetraacetic acid (BAPTA) tetrapotassium salt was added to the pipette solution. The pipette solution for astrocyte dialysis (solution C) contained (in mM): 40 BAPTA, 1 MgCl₂, 10 Hepes, 0.1 EGTA, 0.025 CaCl₂, 1 K₂ATP, 4 glucose, and 0.2 Na₂ GTP. The pH was adjusted to 7.2 with CsOH for solution A and KOH for solutions B and C. All experiments were performed at room temperature (20–22°C). Chemicals were obtained from Sigma-Aldrich or Tocris if not otherwise indicated. Slices were superfused with aCSF and substances were applied by changing the perfusate. When we tested the response of astrocytes to agonists of neurotransmitter receptors, we minimized the indirect effect of neuronal electrical activity by adding TTX (1 µM) to the aCSF. During D-aspartate application 50 µM 6-cyano-7-nitroquinoxaline-2,3-dione (CNQX; an AMPA/kainate receptor [AMPA/KAR] antagonist) and 100 µM DL-2-amino-5-phosphonovaleric acid (APV, an N-methyl-D-aspartate [NMDA] receptor antagonist) were added to the bath solution. To degrade D-serine, slices were incubated for at least 30 min and then continuously perfused with aCSF containing DAO (0.17 U/ml; Sigma-Aldrich). Time-difference histograms of currents were obtained from pair recordings of PPNs. For each event in one half of the pair, we determined the temporally closest event in the other cell. The resulting time differences were used to construct a time-difference histogram similar to that reported previously (Müller et al., 2009). Event pairs occurring in a time window of ±35 ms were considered coincident.

Two-photon microscopy

A two-photon laser-scanning microscope (model BX51WI; Olympus) with a 40x objective was used to detect fluorescent signals (TILL Photonics). A Mira 900 laser (Coherent), tuned to 860 nm, was used for excitation. Image acquisition was controlled by Fluoview FV300 software (Olympus). In the transfluorescence pathway, a 585-nm dichroic mirror was used to separate green and red fluorescence. D510/80M and HQ600LP filters were placed in the “green” and “red” pathways, respectively, to eliminate transmitted or reflected excitation light (Chroma Technology Corp.). For intracellular loading of cells, either lucifer yellow (0.01%) or a combination of Alexa Fluor 568 (0.01%) and Alexa Fluor 594 (0.01%) was used to outline the cell structures.

For 3D reconstruction the inbuilt routine of Fluoview FV300 was used. Afterwards the movie was reduced in display speed with Image-Pro software (ImagePro 5.0, Media Cybernetics and Microcal).

Immunohistochemistry

GFAP-eGFP transgenic mice (8–10-d old) were deeply anesthetized with sodium pentobarbital (100 mg/kg body weight; Sanofi) and perfused intracardially with a solution of 4% paraformaldehyde in 0.1 M phosphate buffer (PB; pH 7.4). Brains were dissected out and postfixed for 2 h at 4°C. After several washes in PB, brains were incubated overnight in 30% sucrose in PB. The next day they were quickly frozen in isopentane, cooled by dry ice. Cryosections (20 µm thick) were mounted on gelatin-coated slides and allowed to dry for 30 min at room temperature. Sections were permeabilized with 0.1% Triton X-100 (TX100) in PB for 20 min and incubated in blocking solution (BS; 0.5% bovine serum albumin, 4% normal goat serum [NGS], 0.01% TX100 in PB) for 1 h at room temperature. Rabbit polyclonal antibodies to GFAP (Dako) were diluted 1:1,000 (in PB/1% bovine serum albumin/1% NGS, 0.01% TX-100). Sections were incubated with the primary antibodies for 24 h at 4°C. Primary antibodies were visualized by application of Alexa 568 goat anti-rabbit IgG (1:2,000; Invitrogen). Secondary antibodies were incubated for 2 h at room temperature. After three washes, sections were mounted with Aquapolymount (Polyscience Inc.) and were inspected in a confocal laser-scanning microscope equipped with a 488-nm argon ion laser (Molecular Dynamics) mounted on an upright microscope (Axioskop; Carl Zeiss, Inc.), as described earlier (Nolte et al., 2001). Specificity of immunoreactivity was controlled by incubation of tissue sections in dilution buffer instead of primary antibodies. In the controls, the immunocytochemical reactions in the CNS were always negative. However, unspecific labeling of the meninges and connective tissue appeared in some cases.

Immunoelectron microscopy

Six GFAP-eGFP-transgenic mice (8–10-d old) were prepared for immunoelectron microscopy, basically as described previously (Nolte et al. 2001). The mice were anesthetized with sodium pentobarbital (100 mg/kg body weight; Sanofi) and perfused transcardially with 4% paraformaldehyde and 0.25% glutaraldehyde in 0.1 M PB (pH 7.3). Brains were removed and postfixed in 4% paraformaldehyde overnight at 4°C. Brains were rinsed in cold PB. 40-µm-thick sagittal sections of the brain stem were cut on a vibratome. For inactivation of endogenous peroxidase, slices were kept in 0.3% H₂O₂ for 15 min at room temperature. Sections were permeabilized with 0.1% Triton X-100 in blocking solution (5% bovine serum albumin and 5% NGS in 0.1 M PB) for 30 min at 4°C. Sections were incubated for 48 h at 4°C with anti-GFP antibodies (A11122 from MoBiTec) at a dilution of 1:500. For negative control, primary antibodies were omitted and slices were incubated in blocking solution. Subsequently, slices were rinsed with cold PB and incubated with peroxidase-conjugated goat anti-rabbit IgG (1:200; Dianova) for 24 h at 4°C. After rinsing, slices were developed using the standard diaminobenzidine (DAB) reaction, postfixed in osmium tetroxide, dehydrated in increasing series of ethanol, preembedded with propylene oxide, and flat-embedded in epoxid resin (agar 100 resin, araldite CY 212, DDSA, DMP-30; Plano). Ultrathin sections were stained with uranyl acetate and lead citrate and examined with an electron microscope (model EM400; Philips) at 80 kV.

Statistics

Statistical analysis was performed using Origin 7.0 software (Origin Laboratories). The results are expressed as mean ± SEM if not otherwise stated. When experiments included a control and more than one test group, data were statistically evaluated with the Tukey test, a probe for ANOVA. We used the Student's *t* test to compare

the two groups (control and test) within an experiment. Here, *P* values <0.05 were considered significant.

Online supplemental material

The online supplemental material contains figures showing synchronized nSICs in a paired neuronal recording (Fig. S1), a raster plot of nSICs evoked after astrocytic calcium response (Fig. S2), bath application of NMDA and NMDA + DAAO on MNTB PPNs (Fig. S3), a video of a 3D reconstruction of an astrocyte completely ensheathing a CoH (Video 1), and a table with the values as depicted in Fig. 7 C (Table S1). Online supplemental material is available at <http://www.jgp.org/cgi/content/full/jgp.200910354/DC1>.

RESULTS

Astrocytes are in contact with several principal neurons in the MNTB

We identified astrocytes using glial fibrillary acidic protein (GFAP)-enhanced GFP (eGFP) transgenic mice (Nolte et al., 2001). Whole-cell recordings revealed that astrocytes had a resting membrane potential of -68 ± 1 mV, a membrane resistance of (*R*_m) of 27 ± 8 MΩ, and a capacitance of 43.6 ± 5.1 pF (*n* = 11). Cells showed passive membrane currents when de- or hyperpolarized between -160 to $+40$ mV (for 50 ms), resulting in a linear current voltage relationship (*n* = 11; Fig. 1, A–C). The peak current at $+40$ mV was 2.8 ± 0.7 nA.

To characterize the potential interaction between astrocytes and the CoH synapse, we studied the morphology of these cells by either dye injection or by inspection of eGFP fluorescence in the GFAP-eGFP transgenic mice (Fig. 1 A; Fig. 2 A). By comparing the number of eGFP-positive cells and PPNs, we found that neurons outnumber the eGFP-positive cells by a factor of 3. Nuclear staining with DAPI allowed us to quantify the total number of somata. We found that $42.9 \pm 1.9\%$ of the cells in the MNTB area were PPNs, $13.0 \pm 1.1\%$ eGFP-positive astrocytes (data collected from 18 slices of 4 animals). Labeling with GFAP antibodies revealed that most eGFP-positive cells were also labeled for GFAP (Fig. 2 B), identifying these cells as astrocytes. We did not observe a complete overlap between eGFP and GFAP. First, not all GFAP-positive cells were eGFP-positive, as described earlier for other areas of the CNS (Nolte et al. 2001). Second, at a subcellular level, GFAP as a cytoskeletal protein was usually observed as bundles in the larger astrocytic processes and in the somata, whereas eGFP was distributed throughout the cell and therefore can be used as a marker at the electron microscopic level to identify the fine astrocytic processes. By inspecting either glial cells with passive membrane currents or eGFP-labeled astrocytes, we found that the cell somata can be in very close contact to the CoH synapse (Fig. 1 A; Fig. 2, A and B), sometimes completely ensheathing the CoH (Video 1), and that a given astrocyte contacted several PPNs with its processes.

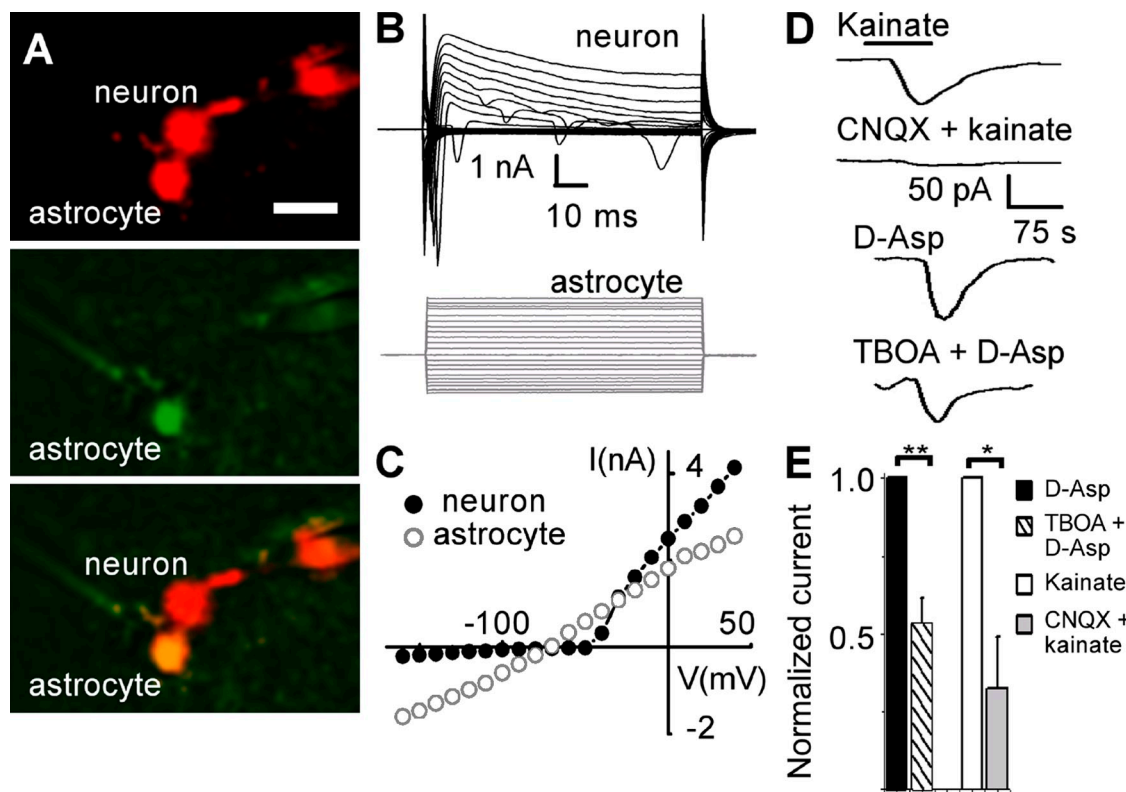


Figure 1. Identification of astrocytes in the MNTB. (A) Fluorescence image showing a principal neuron and a neighboring astrocyte of a GFAP-eGFP mouse, both cells filled with Alexa 594 via the patch pipettes. The top picture shows the red channel, displaying both cells, as well as the tips of both recording pipettes. The middle picture shows the green channel, displaying eGFP fluorescence only in the astrocyte. The bottom picture shows the overlay of eGFP and Alexa fluorescence only in the astrocyte. Bar, 20 μ m (refers to all pictures). (B) Representative current profile. Membrane currents were evoked by 50-ms voltage steps ranging from -160 mV to $+40$ mV, from a holding potential of -70 mV. Note the typical passive response of astrocytes compared with the sodium currents observed in neurons. (C) Current-voltage (IV) relationship from the neuron and the astrocyte shown in B. IV relationship showed a linear pattern in astrocytes and a delayed rectification in neurons. (D) Astrocytes respond to KA and D-Asp. Voltage-clamp recording of an astrocyte clamped to -70 mV. Bath application of KA (0.5 mM) induced inward currents. The response was blocked when CNQX (50 μ M) was preincubated and co-applied with KA (0.5 mM). D-Asp (0.5 mM) elicited an inward current too, this response was reduced when TBOA (100 μ M) was preincubated and co-applied with D-Asp (0.5 mM). The application bars on the top correspond to all applications. (E) Summary of the effect of CNQX on KA and TBOA on D-Asp currents. The amplitudes of KA and D-Asp currents were normalized, showing the relative reduction induced by CNQX ($n = 5$) and TBOA ($n = 6$). Data are the mean \pm SEM. Asterisks represent significant differences (*, $P = 0.01$; **, $P = 0.001$).

GFAP-eGFP-positive astrocytes contact pre- and postsynaptic elements

To obtain detailed information about the morphology of astrocytes and the CoH, GFAP-eGFP transgenic mice were also used to identify astrocytic compartments at the electron microscopic level using antibodies against GFP (Nolte et al., 2001; Jabs et al., 2005). Pre-embedding immunohistochemistry for GFP was performed and ultrathin sections were inspected for labeled astrocytic processes at the ultrastructural level. Labeled processes were frequently found in close proximity to the CoH terminal and were found to directly contact the pre- and postsynaptic membrane (Fig. 2 C). Most importantly, fine astrocytic processes were located at the apposition zone of the finger-like stalks of the CoH and the PPNs (Fig. 2, D and F). Furthermore, fine astrocytic processes were also frequently observed in close vicinity to active zones, the sites of transmitter release and to the puncta

adherentia, desmosome-like structures that connect and stabilize the pre- and postsynaptic membrane (Fig. 2 E; see also Sätzler et al., 2002; Hoffpauir et al., 2006; Rollenhausen and Lübke, 2006). However, no synaptic-like structures between the neuronal elements and the eGFP-labeled processes were observed.

Astrocytes express glutamate transporters and receptors
To test for functional AMPA-KAR in astrocytes, we applied kainic acid (KA; 0.5 mM, 50 s) to the bath while recording membrane currents at a holding potential of -70 mV. KA elicited a small inward current in astrocytes (79 ± 20 pA; $n = 9$). Co-application of KA and the AMPA-KAR antagonist CNQX (50 μ M) reduced the KA-induced current to 20% (16 ± 4 pA; $n = 5$; Fig. 1, D and E). To test for the presence of glutamate transporters, we applied the glutamate transporter agonist D-aspartate (D-Asp; 0.5 mM, 50 s). D-Asp elicited an inward current

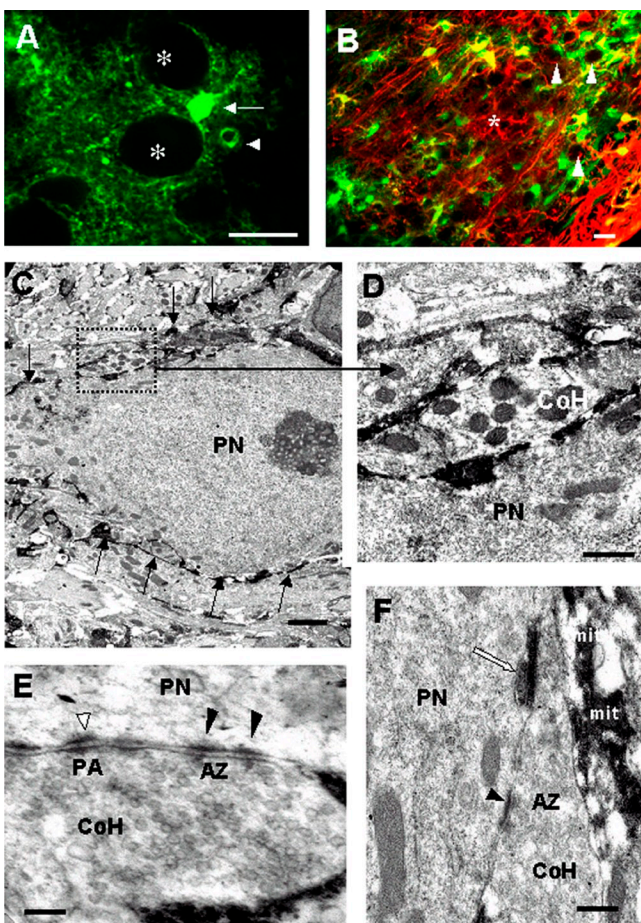


Figure 2. Neurons and astrocytes are in close proximity. (A) Projection image from a stack obtained by two-photon laser-scanning microscopy in a slice of a GFAP-eGFP transgenic animal, showing eGFP-positive astrocytes in the MNTB area. Processes of a single astrocyte (arrow) are in contact with at least two principal neurons (indicated by asterisks). Arrowhead indicates eGFP-positive astrocytic endfeet surrounding a blood vessel. Bar, 20 μ m. (B) Immunolabeling of a vibratome section from an eGFP mouse with GFAP antibodies coupled with Alexa 594 (red); overlay shows that most eGFP-positive cells (green) are also labeled for GFAP (yellow), although there is no complete overlap (asterisk indicates a GFAP-positive cell that is negative for eGFP). Usually the eGFP signal is more pronounced in the cell body, whereas GFAP labeling is more prominent in processes. The principal neurons appear as hollow dark circles (white arrowheads). Note that the amount of GFAP is much higher in close vicinity to the meninges (bottom right corner). Bar, 20 μ m. (C) Overview of an MNTB principal neuron (PN) surrounded by black processes of astrocytes (arrows). (D) Magnified image of outlined area in C. Astrocytes extend their fine processes between the fingers of the calyx of Held (CoH) and the principal neuron (PN). (E and F) Further examples that show how astrocytic processes interdigitate between the fingers of the calyx (CoH) and principal neuron (PN). Black arrowheads indicate active zones (AZ) between a principal neuron and a CoH. Puncta adherentia (PA; white arrowhead) are shown in E. The astrocytic compartments in close vicinity to the calyx contain mitochondria (mit, in F). Note the close apposition of the labeled glial process (white arrow) to the active zone. Bars: (C) 2 μ m; (D–F) 0.2 μ m.

(132 ± 29 pA; $n = 6$; Fig. 1, D and E). Co-application of threo- β -benzyloxyaspartate (TBOA; 100 μ M), a glutamate uptake blocker, reduced the D-Asp-induced current to 58% (77 ± 22 pA; $n = 6$; Fig. 1, D and E). Our results in the mouse MNTB, as demonstrated in the mouse hippocampus (Matthias et al., 2003), support the idea that astrocytes express glutamate transporters and, to a small extent, receptors.

Synaptic activity in the CoH synapse does not elicit uptake currents in astrocytes

We tested the astrocyte response to calyx stimulation by placing a stimulation electrode to the afferent fiber tract at the midline of the brainstem slice and recorded membrane currents from an MNTB astrocyte. A single stimulation pulse did not elicit a response in the astrocyte. Repetitive stimulation with 1 Hz triggered a slow inward current (astrocytic slow inward current [aSIC], 14.6 ± 10.6 pA; decay time constant 6.2 ± 2.7 s; Fig. 3 A). This current was further increased when the stimulation was raised to 10 Hz (41.4 ± 39.1 pA; decay time constant 10.8 ± 7.0 s) or 100 Hz (51.9 ± 53.7 pA; decay time constant 11.8 ± 6.1 s). The aSIC was blocked by TTX (1 μ M) but not by CNQX (50 μ M; not depicted). We then tested the effect of the glutamate transporter antagonist TBOA (200 μ M). TBOA led to an increase in the amplitude of the aSIC by 112.1 ± 31.7 pA (Fig. 3, B and C). This increase was blocked by CNQX (50 μ M) to 36.7 ± 6.7 pA (Fig. 3, B and C). The CNQX-sensitive current had a decay time of 20.22 ± 7.11 s, slower than the inward current recorded in the absence of TBOA (Fig. 3 C). However, when CNQX was added to the aCSF the decay time of the aSIC under TBOA (200 μ M) was reduced to 10.3 ± 6.1 s.

Spontaneous Ca^{2+} responses can be recorded in astrocytes
To record Ca^{2+} activity in astrocytes, slices were loaded with Fluo-4 and astrocytes were identified by using a transgenic animal in which astrocytes express monomeric red fluorescent protein 1 (mRFP1) under the GFAP promoter (Hirrlinger et al., 2005). Spontaneous transient Ca^{2+} responses were observed in $6.5 \pm 8.5\%$ of the astrocytes in the visual field ($n = 74$ astrocytes from 4 experiments; Fig. 4, A and B). The transients lasted for 5–50 s and occurred with a frequency of 2.26 ± 1.60 per min. These transients were observed both in normal aCSF and in aCSF with strychnine and gabazine or aCSF with strychnine, gabazine, CNQX, and AP-5 (Fig. 4, A and B).

Slow inward currents can be recorded in MNTB principal neurons

NMDA-mediated nSICs have been linked to glutamate release from astrocytes (D'Ascenzo et al., 2007). In some cases, we observed nSICs, but such events were rare under normal aCSF. Therefore, we used a solution with low extracellular magnesium and low extracellular calcium

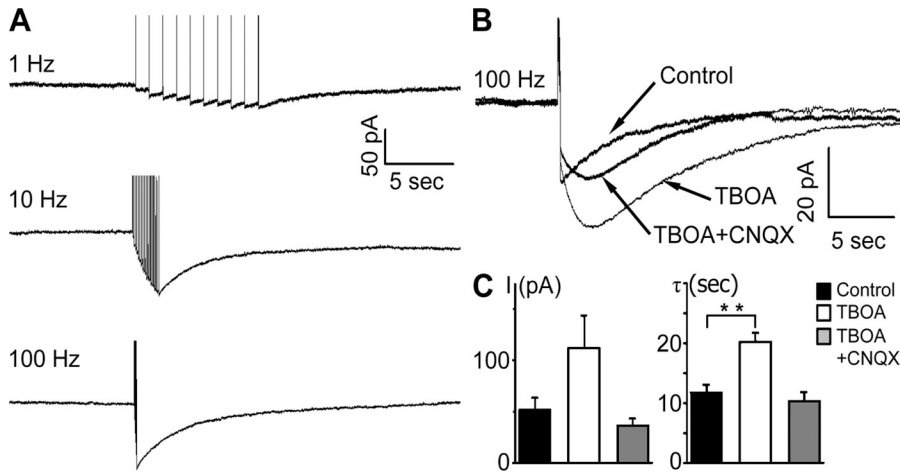


Figure 3. Tetanic stimulation reveals slow inward currents in the astrocytes (asICs). (A) Currents recorded from astrocytes in response to midline stimulation with 10 pulses at 1 Hz (top), 20 pulses at 10 Hz (middle), and 20 pulses at 100 Hz (bottom). (B) Currents recorded in response to midline stimulation with 20 pulses at 100 Hz. Overlay of three consecutive records from the same cell. Inhibition of glutamate transporters with TBOA (200 μ M) results in an increase of the current as compared with control. Application of TBOA (200 μ M) and CNQX (20 μ M) results in a reduction of the current to almost control value. (C) Summary of the current amplitudes and the decay times of the current induced by 20 pulses at 100 Hz under control conditions, under TBOA and under TBOA together with CNQX ($n = 21$). Data are the mean \pm SEM. Asterisks represent significant difference (**, $P = 0.002$).

to promote the opening of NMDA receptors (Fellin et al., 2007) and calcium signals in astrocytes (Stout and Charles, 2003). These conditions facilitated the occurrence of nSICs. Indeed, in low calcium and magnesium solution, nSICs were recorded in 46% of the PPNs of the MNTB ($n = 46$ recorded neurons). These currents were observed at a low frequency (0.275 ± 0.056 events/min; Fig. 5 A). The mean amplitude of nSICs was 89.3 ± 9.7 pA (97 events; ranging from 15 pA to 540 pA; Fig. 5, C and D). The miniature excitatory postsynaptic currents (mEPSCs; Fig. 5, A and B) displayed a faster decay time constant (1.85 ± 0.59 ms; Müller et al., 2009) than nSICs (166.6 ± 16.3 ms; ranging from 40 to 960 ms; Fig. 5, A–D). Both types of currents can be recorded in the same neuron (Fig. 5 A). We conclude that the decay time constant is a valid kinetic parameter to distinguish nSICs from mEPSCs.

Spontaneous slow inward currents in principal neurons disappear when interfering with astrocyte calcium signaling

Paired recordings of a PPN and an adjacent astrocyte were performed to study the involvement of astrocytic calcium signaling in nSICs. Astrocytes were dialyzed with BAPTA via the patch pipette (40 mM) to inhibit astrocytic calcium signaling. Normal aCSF was alternated with a low calcium and magnesium solution in periods of 5 min during the recording time (between 45 and 60 min). The nSICs were never observed when the astrocyte and the neuron were <20 μ m apart ($n = 6$; Fig. 6, A and B).

As reported in an earlier study, astrocytes in the MNTB are coupled via gap junctions (Müller et al., 2009). However, the spread of BAPTA via gap junctions is limited

within the astrocyte syncytium (Serrano et al., 2006). Thus, we conducted a series of experiments where an astrocyte was filled with BAPTA and currents were recorded from neighboring PPNs at different distances from the patched astrocyte. We observed only 1 nSIC in 6 PPNs (16.6%) when the neuron was 20–50 μ m away from the filled astrocyte (Fig. 6 B). In contrast, nSICs were recorded in 4 out of 6 PPNs (66.6%) when the neuron was >50 μ m away from the astrocyte, supporting the idea that the spread of BAPTA is limited (Fig. 6 B). These results support the hypothesis that calcium activity in MNTB astrocytes triggers nSICs in PPNs due to release of a gliotransmitter.

Synchrony of nSICs in PPNs is rarely observed

Studies in the hippocampus and nucleus accumbens suggest that astrocytic glutamate release mediates synchronous activation of nSICs in different neurons (Fellin et al., 2004; D'Ascenzo et al., 2007). We performed whole-cell paired recordings of PPNs (<50 μ m of distance) in low calcium and magnesium saline ($n = 12$ paired recordings) to test for synchronous activation of nSICs. A total of 50 nSICs was observed and the majority were noncoincident events ($n = 46$ nSICs; Fig. 7, A and B); only 4 coincident nSICs were recorded in two cell pairs ($n = 12$ paired recordings; Fig. S1). These results suggest that, in contrast to the hippocampus or nucleus accumbens, synchrony of PPNs in MNTB is not common.

Calcium responses in astrocytes correlate with an increased frequency of nSICs

Electrical stimulation in the MNTB evoked calcium responses in astrocytes while neuronal activity was blocked by TTX (Fig. 8, A and B). Therefore, we tested if the probability to observe nSICs increased after an

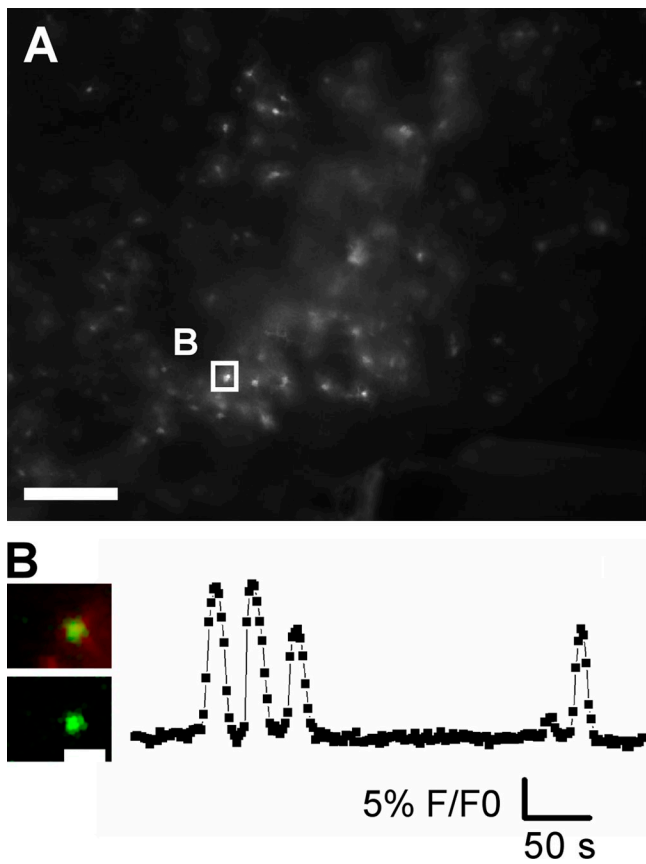


Figure 4. Spontaneous calcium signals in MNTB astrocytes. (A) Overview of the MNTB region of a GFAP-mRFP1 transgenic mouse brainstem slice showing mRFP1 fluorescence. Bar, 200 μ m. (B) On the left, a cell (marked by a box in A) is displayed in higher magnification. The top image is the overlay of mRFP1 expression and Fluo-4 staining, the bottom image is the Fluo-4 staining alone. Bar, 20 μ m. On the right, the Fluo-4 fluorescence change (F/F_0) from that cell is shown.

evoked glial calcium response in a 100-s window time (Fig. 8, A and B; see Materials and methods). Experiments with normal aCSF showed an apparent increase in the probability to observe nSICs before stimulation and after stimulation, but this increase was not significant (0.015 ± 0.010 vs. 0.058 ± 0.037 ; $n = 16$, $P = 0.27$; Fig. 8 C). Addition of TTX (1 μ M) to the aCSF increased the probability to observe nSICs after stimulation (0.011 ± 0.011 vs. 0.097 ± 0.037 ; $n = 16$, $P = 0.036$; Fig. 8 C). A similar effect was observed in Mg^{2+} -free aCSF + TTX (1 μ M) (0.015 ± 0.010 vs. 0.093 ± 0.050 ; $n = 17$, $P = 0.13$; Fig. 8 C). However, a prominent increase in nSICs occurred after astrocyte stimulation when strychnine (1 μ M) and gabazine (10 μ M) were added to the Mg^{2+} -free aCSF + TTX (1 μ M) (0.022 ± 0.012 vs. 0.3 ± 0.1 ; $n = 20$, $P = 0.0089$; Fig. 8 C, Fig. S2). Based on these results, Mg^{2+} -free aCSF + strychnine + gabazine was used for further experiments. In the presence of CNQX (25 μ M), the increase in the probability to record an nSIC after stimulation was still

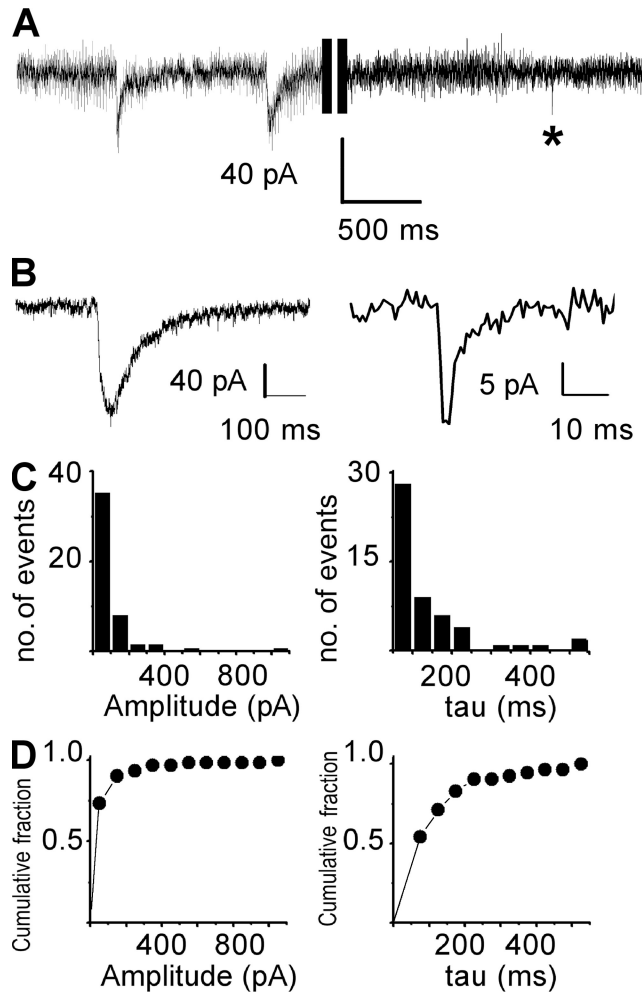


Figure 5. nSICs evoked in PPNs of the MNTB under aCSF without Mg^{2+} and Ca^{2+} . (A) Whole-cell voltage-clamp recording from a PPN showing spontaneous nSICs ($n = 97$ nSICs from 46 neurons) and an mEPSC (asterisk). (B) Representative nSIC (right) and mEPSC (left) recorded in aCSF with TTX (1 μ M), strychnine (1 μ M), and gabazine (10 μ M). (C) Histogram showing amplitude (left) and decay time constant (τ , right) of the recorded nSICs. (D) Cumulative fraction plots of nSICs for amplitude and decay time constant.

observed (no events before stimulation vs. 0.179 ± 0.066 after stimulation; $n = 24$, $P = 0.0094$; Fig. 8 C). However, nSICs were almost completely blocked by ifenprodil (100 μ M), an antagonist of NMDA receptors containing the subunit NR2B, co-applied with CNQX (25 μ M) (no events before stimulation vs. 0.006 ± 0.004 after stimulation; $n = 17$, $P = 0.15$; Fig. 8 C). A similar effect was observed when the NMDA receptor antagonists MK-801 (10 μ M) + APV (50 μ M) were used, together with TTX (1 μ M) in Mg^{2+} -free aCSF + strychnine + gabazine (not depicted).

D-serine is considered a gliotransmitter released by astrocytes acting as a co-agonist on NMDA receptors (Panatier et al., 2006). Therefore, we tested the effect of D-amino acid oxidase (DAAO), a D-serine degrading

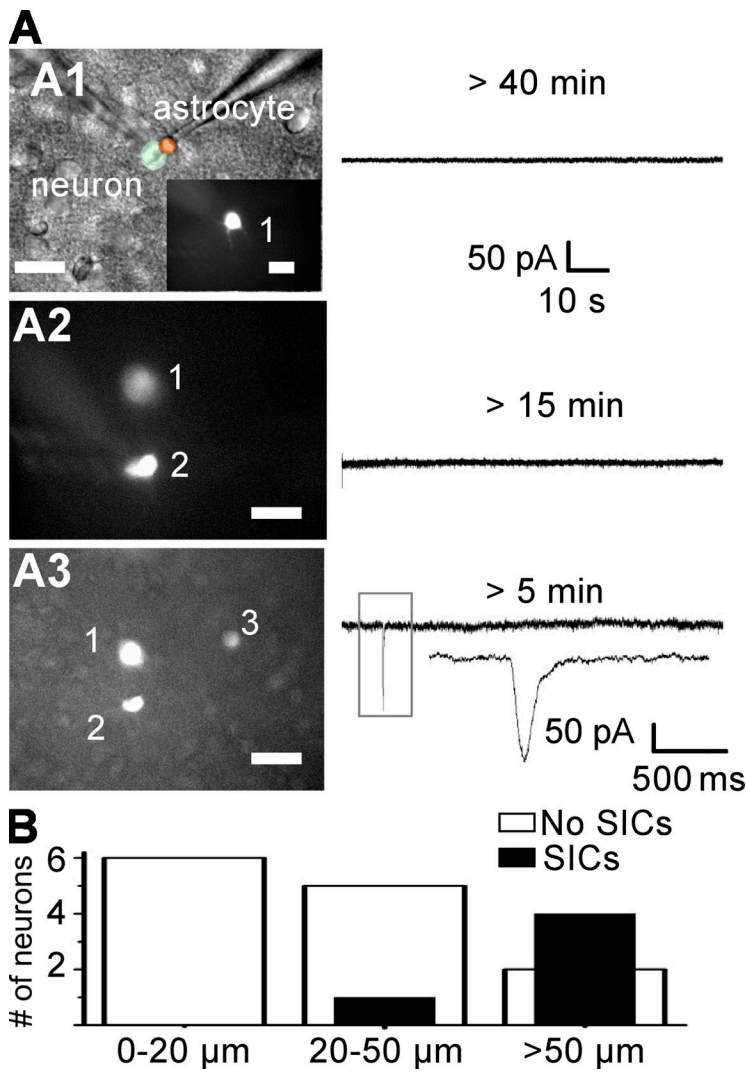


Figure 6. Gliotransmission evokes nSICs in PPNs. (A and A1) Representative paired recording of astrocyte and PPN. Both types of cells were identified morphologically and based on their current profile. aCSF without Ca^{2+} and Mg^{2+} + TTX (1 μM) was used to promote the appearance of nSICs. Astrocytes were dialyzed with 40 mM BAPTA through the pipette and continuous recording of neuron (black trace) and astrocyte were performed for 45–60 min. No nSICs were observed under these experimental conditions ($n = 6$). (A2) A second neuron was patched after dialysis of the astrocyte (>45 min). This neuron was 20–50 μm away from the original pair recording. Note that no nSICs were observed. (A3) A third neuron located to the right of the original pair recording (>50 μm) showed a nSIC. (B) Summary of nSICs recorded in 3 different neurons (in the same slice) during and after astrocyte dialysis with BAPTA.

enzyme (0.17 U/ml; see Materials and methods), on nSIC frequency. DAAO reduced the probability to observe nSICs (0.04 ± 0.018 before vs. 0.0096 ± 0.0056 after stimulation; $n = 15$, $P = 0.71$; Fig. 8 C). To confirm that D-serine participates in NMDA-mediated currents we bath applied NMDA to PPNs. NMDA (100 μM , co-applied with 1 μM TTX, 1 μM strychnine, and 10 μM gabazine) elicited an inward current of 135.15 ± 28.77 pA ($n = 10$). Incubation of slices with DAAO reduced the inward currents to 55% of the original response (74.56 ± 17.22 pA; $n = 9$; Fig. S3). This led to the interpretation that D-serine acts as a co-agonist at the NMDA receptors in the MNTB.

To further demonstrate that nSICs were astrocyte mediated, we recorded from an astrocyte and injected BAPTA to interfere with calcium excitability. This strategy showed to be effective because the probability to observe nSICs was dramatically reduced (no events before stimulation vs. 0.015 after stimulation; $n = 8$, $P = 0.33$; Fig. 8 C; see Table S1 to compare all the values). Collectively, our results indicate that neurons respond to astrocyte activity via activation of NMDA receptors.

DISCUSSION

At the CoH synapse, similar to other brain regions, astrocytes are in close apposition with neurons, and synapses are often ensheathed by astrocytic processes (Schikorski and Stevens, 1997; Grosche et al., 2002; Sätzler et al., 2002; Renden et al., 2005; Müller et al., 2009). Our light and electron microscopic studies revealed that thin astrocytic processes are in contact with both the membrane of calyx and postsynaptic neuron. We further provided evidence that astrocyte activity elicited responses in the postsynaptic neuron in the form of slow inward currents.

Calyx activity does not trigger glutamate uptake currents in astrocytes

Immunocytochemical and electron microscopy studies showed glutamate aspartate transporter (GLAST) expression in glial processes contacting PPN and CoH (Renden et al., 2005). We recorded a current response when we applied D-Asp, a substrate for glutamate transporters, and

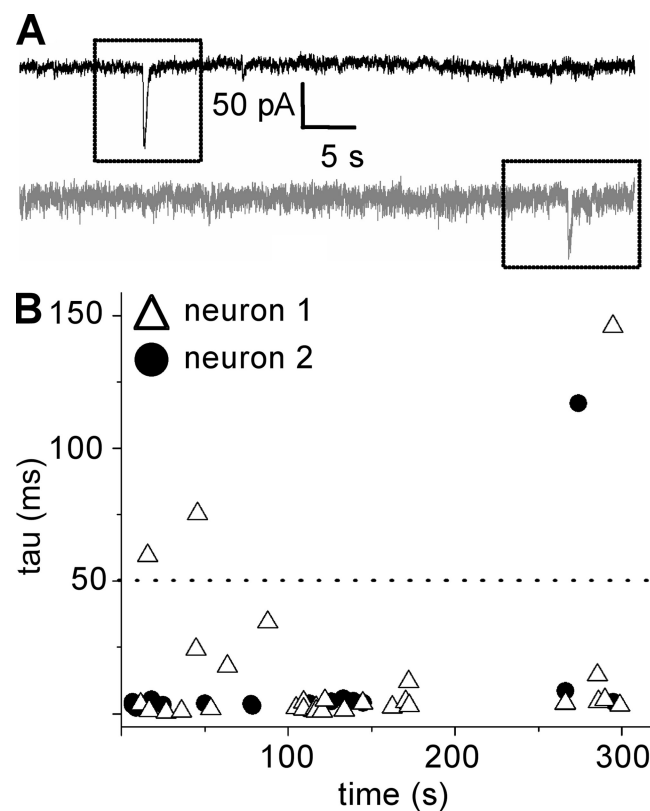


Figure 7. Synchrony of nSICs in PPNs is rarely observed. (A) Neuronal paired recording where synchrony of nSICs is absent ($n = 10$ out of 12 paired recordings). The paired recording was obtained in aCSF with low Ca^{2+} and Mg^{2+} + TTX (1 μM) + strychnine (1 μM) + gabazine (10 μM). (B) Raster plot of a representative neuronal paired recording showing the decay time constant (τ) and time of occurrence of the events recorded in 300 s. A total of 49 events was recorded (events observed in neuron 1 [Δ ; 30 events] or neuron 2 [\bullet ; 19 events]).

this current was partially blocked by TBOA. In the hippocampus and in the cerebellum, activation of glutamatergic synapses triggers current responses in astrocytes, which are due to the activity of electrogenic glutamate transporters (Bergles et al., 1999). However, we did not observe uptake currents correlated with the electrical stimulation of presynaptic fibers in astrocytes from the MNTB. Thus, we think that the glutamate uptake occurs only at the far tip of thin processes and that the resulting current cannot be recorded in the soma of the cell. On the other hand, the processes of Bergmann glial cells show even a higher arborization and glutamate uptake currents can be reliably recorded (Bergles et al., 1997). Nevertheless, glial transporters in the MNTB are excluded from the synaptic cleft and are not essential for controlling the postsynaptic response at a given CoH terminal, explaining why we did not observe stimulus-evoked uptake currents (Renden et al., 2005). The authors perceive that glutamate transporters in the MNTB act as barriers between synapses and thereby influence the activity of calyceal metabotropic glutamate receptors (Renden et al., 2005).

The slow inward currents recorded in the astrocytes in response to repetitive midline stimulation are most likely due to an increase in extracellular potassium. It is well established that neuronal activity leads to an increase in potassium in the extracellular space. Neuronal activity triggering increases in potassium by several mM have been reported in many brain regions (for review see Syková and Nicholson, 2008). Because astrocytes have a high potassium conductance with linear current to voltage relationship, the increase in extracellular potassium leads to a depolarization or, when voltage clamped, to an inward current. All our observations would fit this explanation: (1) the current increased with an increase in frequency of stimulation; (2) the current is sensitive to TTX; and (3) the current is increased by the glutamate transporter blocker TBOA. The latter is due to an increased availability of glutamate at the synapse, thereby leading to an increased activation of glutamate receptors and postsynaptic depolarization/activity. It also explains why this increase is blocked by CNQX. Likewise, an analogue slow inward current was observed in astrocytes from the hippocampus that was blocked by kynurenic acid or treatment with K^+ channel blockers (Ge et al., 2006; Ge and Duan, 2007).

A similar current response has also been observed in Bergmann glial cells in response to parallel fiber activation. This current was blocked by inhibition of G proteins and it has been speculated that the response could be due to the release of an unknown substance from neurons activating G protein–coupled receptors in the glial cells (Bellamy and Ogden, 2005).

nSICs in principal neurons depend on astrocyte activity

The functional expression of NMDA receptors in PPNs of the MNTB reaches a peak during postnatal day 11/12 and declines to very low levels after postnatal day 16 (Joshi and Wang, 2002). During this developmental window, NMDA-mediated EPSCs can be evoked by calyceal or noncalyceal inputs (Joshi and Wang, 2002; Hamann et al., 2003). Both inputs are abolished when TTX is added to the extracellular solution (Hamann et al., 2003; Müller et al., 2009). We now report that gliotransmission evokes NMDA-mediated nSICs in PPNs of the MNTB. Similar currents have been reported for the hippocampus and the nucleus accumbens (Fellin et al., 2007). Although vesicular release of glutamate and glycine from calyceal and noncalyceal inputs can still occur under TTX, removal of calcium from aCSF further compromises neuronal transmission. On the other hand, calcium removal from aCSF is known to promote transient intracellular calcium increases in astrocytes, a necessary step to evoke gliotransmission (Stout and Charles, 2003). Interestingly, we found that the frequency of nSICs was increased when strychnine and gabazine, blockers of glycine and GABA_A receptors, were added. In the CoH, glycine increases while presynaptic

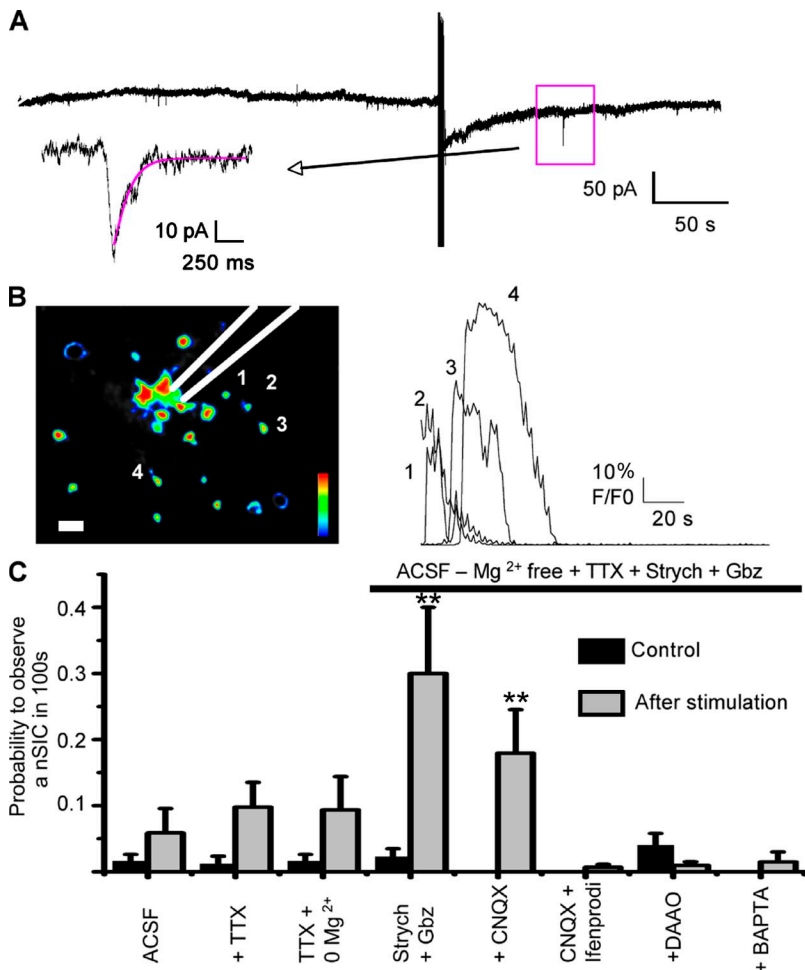


Figure 8. Whole-cell recording from a PPN before and after a calcium wave evoked by electrical stimulation. (A) PPNs were recorded under different experimental conditions. nSICs recorded 100 s before and 100 s after an evoked calcium response were used for analysis. Preincubation with the aCSF (alone, modified, or modified + drugs) was always performed. The calcium response was evoked with current pulses (100 μ A) at 10 Hz in 4 s. Square shows an nSIC after stimulation. Arrow shows magnification of the recorded nSIC. (B) Calcium response evoked by electrical stimulation. Left: false-color image of the MNTB region. Numbers 1–4 show some active astrocytes. The position of the stimulation electrode is illustrated. Right: calcium responses (F/F_0) of the four astrocytes indicated on the left. (C) Summary of nSICs before and after stimulation in aCSF ($n = 16$); aCSF + TTX (1 μ M) ($n = 16$); Mg²⁺-free aCSF; Mg²⁺-free aCSF + TTX (1 μ M) ($n = 17$); Mg²⁺-free aCSF + strychnine (1 μ M) + gabazine (10 μ M) + TTX (1 μ M) ($n = 20$); Mg²⁺-free aCSF + strychnine (1 μ M) + gabazine (10 μ M) + CNQX (25 μ M) + TTX (1 μ M) ($n = 24$); Mg²⁺-free aCSF + strychnine (1 μ M) + gabazine (10 μ M) + CNQX (25 μ M) + ifenprodil (100 μ M) ($n = 17$) + TTX (1 μ M); Mg²⁺-free aCSF + strychnine (1 μ M) + gabazine (10 μ M) + DAAO + TTX (1 μ M) ($n = 15$); and Mg²⁺-free aCSF + strychnine (1 μ M) + gabazine + TTX (1 μ M) in a slice where an astrocyte was dialyzed with BAPTA 20 min before ($n = 8$). See the text and Table S1 for values.

GABA_B receptors suppress transmitter release (Isaacson, 1998; Takahashi et al., 1998; Turecek and Trussell, 2001). Thus, the block of GABA_A receptor with gabazine might promote GABA_B receptor activation, and therefore block of glycine and GABA_A receptors will reduce glutamate release from CoH. Nevertheless, gliotransmission could be promoted through activation of astrocyte GABA_B receptors (Kang et al., 1998; Serrano et al., 2006). We think that this could explain why nSICs frequency increase when gabazine and strychnine are added to the aCSF.

As in previous studies, we were able to block nSICs in the MNTB with APV, MK-801, or ifenprodil in combination with CNQX. Ifenprodil is known to block the NR2B2 subunit and in the MNTB blocks $\sim 25\%$ of principal NMDA currents (Joshi and Wang, 2002). We assume that nSICs are mediated by ifenprodil-sensitive NMDA currents and conclude that nSICs in PPNs of the MNTB are due to the activation of NMDA receptors containing the NR2B2 subunit.

The nSICs in the PPNs are evoked by astrocytic activity and this is supported by the following observations: (1) nSICs were completely absent when astrocytes in the vicinity of the neuron were dialyzed with BAPTA; and (2)

after eliciting a Ca²⁺ response in astrocytes, the frequency of nSICs increased. These results are in agreement with observations made in the hippocampus and nucleus accumbens where nSICs are mediated by NMDA receptors containing the NR2B2 subunit (Angulo et al., 2004; Fellin et al., 2004; D'Ascenzo et al., 2007; Shigetomi et al., 2008). Likewise, and similar to studies in the supraoptic nucleus in the hypothalamus (Panatier et al., 2006), our data suggest that D-serine is co-released with glutamate because degradation of D-serine with DAAO led to a significant decrease of nSICs. In addition, DAAO significantly reduced NMDA-evoked currents (Fig. S3), suggesting that D-serine acts as a co-agonist at NMDA receptors. Because D-serine is solely released by astrocytes (Panatier et al., 2006), we conclude that astrocytes are mainly responsible for the nSICs. Our results are in agreement with previous studies in other brain regions (Angulo et al., 2004; Fellin et al., 2004; D'Ascenzo et al., 2007).

D-serine as a possible co-agonist of NMDA-mediated nSICs

The NMDA receptors play a key role during postnatal development of the MNTB (Joshi and Wang, 2002). Glycine or D-serine are required co-agonists for NMDA

activation and consequently of nSICs. In this study we explore D-serine as a possible co-agonist of NMDA-mediated nSICs. This hypothesis is supported by previous evidence in the brainstem. First, glycinergic activity reaches a peak only after 2 wk of postnatal development of the MNTB (Awatramani et al., 2005). Second, D-serine levels increase during postnatal development and start to decrease when DAAO expression begins, 2 wk after postnatal development of the brainstem and cerebellum (Hashimoto et al., 1995; Horiike et al., 2001; Wang and Zhu, 2003). Moreover, the regional D-serine content correlates with the distribution of NMDA receptors in the rat brain (Schell et al., 1995, 1997). Our results show that incubation of brainstem slices with DAAO significantly reduces the probability to observe NMDA-mediated nSICs. Moreover, extracellular application of NMDA resulted in a reduced response in PPNs of the MNTB when DAAO is present, supporting D-serine as co-agonist of NMDA receptors. Thus, considering our results and the role of D-serine and glycine during postnatal development, we propose that D-serine is involved in NMDA-mediated nSICs. Overall, we conclude that gliotransmission through astrocytes occurs at the CoH synapse. Specifically, astrocytes signal to PPNs where they activate NMDA-mediated nSICs.

nSICs and development of the auditory system

The PPNs of the MNTB project to the lateral superior olive where they establish inhibitory synapses. During development of the auditory system, NMDA receptors play a key role in the functional refinement of inhibitory synapses (Kim and Kandler, 2003; Kandler, 2004). Accordingly, our results indicate that gliotransmission is an additional element to consider in the development and plasticity of the auditory system.

We are grateful to Rainer Kroeber, Irene Haupt, and Birgit Jarchow for technical assistance.

This study was supported by a grant from the Deutsche Forschungsgemeinschaft (SPP 1172).

Submitted: 27 October 2009

Accepted: 31 March 2010

REFERENCES

- Angulo, M.C., A.S. Kozlov, S. Charpak, and E. Audinat. 2004. Glutamate released from glial cells synchronizes neuronal activity in the hippocampus. *J. Neurosci.* 24:6920–6927. doi:10.1523/JNEUROSCI.0473-04.2004
- Awatramani, G.B., R. Turecek, and L.O. Trussell. 2005. Staggered development of GABAergic and glycinergic transmission in the MNTB. *J. Neurophysiol.* 93:819–828. doi:10.1152/jn.00798.2004
- Barnes-Davies, M., and I.D. Forsythe. 1995. Pre- and postsynaptic glutamate receptors at a giant excitatory synapse in rat auditory brainstem slices. *J. Physiol.* 488:387–406.
- Bellamy, T.C., and D. Ogden. 2005. Short-term plasticity of Bergmann glial cell extrasynaptic currents during parallel fiber stimulation in rat cerebellum. *Glia.* 52:325–335. doi:10.1002/glia.20248
- Bergles, D.E., J.A. Dzubay, and C.E. Jahr. 1997. Glutamate transporter currents in Bergmann glial cells follow the time course of extrasynaptic glutamate. *Proc. Natl. Acad. Sci. USA.* 94:14821–14825. doi:10.1073/pnas.94.26.14821
- Bergles, D.E., J.S. Diamond, and C.E. Jahr. 1999. Clearance of glutamate inside the synapse and beyond. *Curr. Opin. Neurobiol.* 9:293–298. doi:10.1016/S0959-4388(99)80043-9
- D'Ascenzo, M., T. Fellin, M. Terunuma, R. Revilla-Sanchez, D.F. Meaney, Y.P. Auberson, S.J. Moss, and P.G. Haydon. 2007. mGluR5 stimulates gliotransmission in the nucleus accumbens. *Proc. Natl. Acad. Sci. USA.* 104:1995–2000. doi:10.1073/pnas.0609408104
- Elezgarai, I., A. Bilbao, J.M. Mateos, J.J. Azkue, R. Benítez, A. Osorio, J. Díez, N. Puente, F. Doñate-Oliver, and P. Grandes. 2001. Group II metabotropic glutamate receptors are differentially expressed in the medial nucleus of the trapezoid body in the developing and adult rat. *Neuroscience.* 104:487–498. doi:10.1016/S0306-4522(01)00080-X
- Fellin, T., O. Pascual, S. Gobbo, T. Pozzan, P.G. Haydon, and G. Carmignoto. 2004. Neuronal synchrony mediated by astrocytic glutamate through activation of extrasynaptic NMDA receptors. *Neuron.* 43:729–743. doi:10.1016/j.neuron.2004.08.011
- Fellin, T., M. D'Ascenzo, and P.G. Haydon. 2007. Astrocytes control neuronal excitability in the nucleus accumbens. *ScientificWorldJournal.* 7:89–97.
- Forsythe, I.D. 1994. Direct patch recording from identified presynaptic terminals mediating glutamatergic EPSCs in the rat CNS, *in vitro*. *J. Physiol.* 479:381–387.
- Ge, W.P., and S. Duan. 2007. Persistent enhancement of neuron-glia signaling mediated by increased extracellular K⁺ accompanying long-term synaptic potentiation. *J. Neurophysiol.* 97:2564–2569. doi:10.1152/jn.00146.2006
- Ge, W.P., X.J. Yang, Z. Zhang, H.K. Wang, W. Shen, Q.D. Deng, and S. Duan. 2006. Long-term potentiation of neuron-glia synapses mediated by Ca²⁺-permeable AMPA receptors. *Science.* 312:1533–1537. doi:10.1126/science.1124669
- Grosche, J., H. Kettenmann, and A. Reichenbach. 2002. Bergmann glial cells form distinct morphological structures to interact with cerebellar neurons. *J. Neurosci. Res.* 68:138–149. doi:10.1002/jnr.10197
- Hamann, M., B. Billups, and I.D. Forsythe. 2003. Non-calyceal excitatory inputs mediate low fidelity synaptic transmission in rat auditory brainstem slices. *Eur. J. Neurosci.* 18:2899–2902. doi:10.1111/j.1460-9568.2003.03017.x
- Hamill, O.P., A. Marty, E. Neher, B. Sakmann, and F.J. Sigworth. 1981. Improved patch-clamp techniques for high-resolution current recording from cells and cell-free membrane patches. *Pflugers Arch.* 391:85–100. doi:10.1007/BF00656997
- Hashimoto, A., T. Oka, and T. Nishikawa. 1995. Extracellular concentration of endogenous free D-serine in the rat brain as revealed by *in vivo* microdialysis. *Neuroscience.* 66:635–643. doi:10.1016/0306-4522(94)00597-X
- Hirrlinger, P.G., A. Scheller, C. Braun, M. Quintela-Schneider, B. Fuss, J. Hirrlinger, and F. Kirchhoff. 2005. Expression of reef coral fluorescent proteins in the central nervous system of transgenic mice. *Mol. Cell. Neurosci.* 30:291–303. doi:10.1016/j.mcn.2005.08.011
- Hoffpauir, B.K., J.L. Grimes, P.H. Mathers, and G.A. Spirou. 2006. Synaptogenesis of the calyx of Held: rapid onset of function and one-to-one morphological innervation. *J. Neurosci.* 26:5511–5523. doi:10.1523/JNEUROSCI.5525-05.2006
- Horiike, K., T. Ishida, H. Tanaka, and R. Arai. 2001. Distribution of D-amino acid oxidase and D-serine in vertebrate brains. *J. Mol. Catal., B Enzym.* 12:37–41. doi:10.1016/S1381-1177(00)00201-0
- Isaacson, J.S. 1998. GABAB receptor-mediated modulation of presynaptic currents and excitatory transmission at a fast central synapse. *J. Neurophysiol.* 80:1571–1576.
- Jabs, R., T. Pivneva, K. Hüttmann, A. Wyczynski, C. Nolte, H. Kettenmann, and C. Steinhäuser. 2005. Synaptic transmission

- onto hippocampal glial cells with hGFAP promoter activity. *J. Cell Sci.* 118:3791–3803. doi:10.1242/jcs.02515
- Joshi, I., and L.Y. Wang. 2002. Developmental profiles of glutamate receptors and synaptic transmission at a single synapse in the mouse auditory brainstem. *J. Physiol.* 540:861–873. doi:10.1113/jphysiol.2001.013506
- Jourdain, P., L.H. Bergersen, K. Bhaukaurally, P. Bezzi, M. Santello, M. Domercq, C. Matute, F. Tonello, V. Gundersen, and A. Volterra. 2007. Glutamate exocytosis from astrocytes controls synaptic strength. *Nat. Neurosci.* 10:331–339. doi:10.1038/nn1849
- Kandler, K. 2004. Activity-dependent organization of inhibitory circuits: lessons from the auditory system. *Curr. Opin. Neurobiol.* 14:96–104. doi:10.1016/j.conb.2004.01.017
- Kang, J., L. Jiang, S.A. Goldman, and M. Nedergaard. 1998. Astrocyte-mediated potentiation of inhibitory synaptic transmission. *Nat. Neurosci.* 1:683–692. doi:10.1038/3684
- Katz, B., and R. Miledi. 1965. The effect of calcium on acetylcholine release from motor nerve terminals. *Proc R Soc Lond B Biol Sci.* 161:496–503. doi:10.1098/rspb.1965.0017
- Kim, G., and K. Kandler. 2003. Elimination and strengthening of glycinergic/GABAergic connections during tonotopic map formation. *Nat. Neurosci.* 6:282–290. doi:10.1038/nn1015
- Kuwabara, N., R.A. DiCaprio, and J.M. Zook. 1991. Afferents to the medial nucleus of the trapezoid body and their collateral projections. *J. Comp. Neurol.* 314:684–706. doi:10.1002/cne.903140405
- Matthias, K., F. Kirchhoff, G. Seifert, K. Hüttmann, M. Matyash, H. Kettenmann, and C. Steinhäuser. 2003. Segregated expression of AMPA-type glutamate receptors and glutamate transporters defines distinct astrocyte populations in the mouse hippocampus. *J. Neurosci.* 23:1750–1758.
- Miledi, R. 1973. Transmitter release induced by injection of calcium ions into nerve terminals. *Proc R Soc Lond B Biol Sci.* 183:421–425. doi:10.1098/rspb.1973.0026
- Müller, J., D. Reyes-Haro, T. Pivneva, C. Nolte, R. Schaeffer, J. Lübke, and H. Kettenmann. 2009. The principal neurons of the medial nucleus of the trapezoid body and NG2(+) glial cells receive coordinated excitatory synaptic input. *J. Gen. Physiol.* 134:115–127. doi:10.1085/jgp.200910194
- Navarrete, M., and A. Araque. 2008. Endocannabinoids mediate neuron-astrocyte communication. *Neuron.* 57:883–893. doi:10.1016/j.neuron.2008.01.029
- Nolte, C., M. Matyash, T. Pivneva, C.G. Schipke, C. Ohlemeyer, U.K. Hanisch, F. Kirchhoff, and H. Kettenmann. 2001. GFAP promoter-controlled EGFP-expressing transgenic mice: a tool to visualize astrocytes and astrogliosis in living brain tissue. *Glia.* 33:72–86. doi:10.1002/1098-1136(20010101)33:1<72::AID-GLIA1007>3.0.CO;2-A
- Panatier, A., D.T. Theodosis, J.P. Mothet, B. Touquet, L. Pollegioni, D.A. Poulain, and S.H. Oliet. 2006. Glia-derived D-serine controls NMDA receptor activity and synaptic memory. *Cell.* 125:775–784. doi:10.1016/j.cell.2006.02.051
- Perea, G., and A. Araque. 2007. Astrocytes potentiate transmitter release at single hippocampal synapses. *Science.* 317:1083–1086. doi:10.1126/science.1144640
- Renden, R., H. Taschenberger, N. Puente, D.A. Rusakov, R. Duvoisin, L.Y. Wang, K.P. Lehre, and H. von Gersdorff. 2005. Glutamate transporter studies reveal the pruning of metabotropic glutamate receptors and absence of AMPA receptor desensitization at mature calyx of held synapses. *J. Neurosci.* 25:8482–8497. doi:10.1523/JNEUROSCI.1848-05.2005
- Rollenhagen, A., and J.H. Lübke. 2006. The morphology of excitatory central synapses: from structure to function. *Cell Tissue Res.* 326:221–237. doi:10.1007/s00441-006-0288-z
- Sätzler, K., L.F. Söhl, J.H. Bollmann, J.G. Borst, M. Frotscher, B. Sakmann, and J.H. Lübke. 2002. Three-dimensional reconstruction of a calyx of Held and its postsynaptic principal neuron in the medial nucleus of the trapezoid body. *J. Neurosci.* 22:10567–10579.
- Schell, M.J., M.E. Molliver, and S.H. Snyder. 1995. D-serine, an endogenous synaptic modulator: localization to astrocytes and glutamate-stimulated release. *Proc. Natl. Acad. Sci. USA.* 92:3948–3952. doi:10.1073/pnas.92.9.3948
- Schell, M.J., R.O. Brady Jr., M.E. Molliver, and S.H. Snyder. 1997. D-serine as a neuromodulator: regional and developmental localizations in rat brain glia resemble NMDA receptors. *J. Neurosci.* 17:1604–1615.
- Schikorski, T., and C.F. Stevens. 1997. Quantitative ultrastructural analysis of hippocampal excitatory synapses. *J. Neurosci.* 17:5858–5867.
- Schneggenburger, R., and I.D. Forsythe. 2006. The calyx of Held. *Cell Tissue Res.* 326:311–337. doi:10.1007/s00441-006-0272-7
- Serrano, A., N. Haddjeri, J.C. Lacaille, and R. Robitaille. 2006. GABAergic network activation of glial cells underlies hippocampal heterosynaptic depression. *J. Neurosci.* 26:5370–5382. doi:10.1523/JNEUROSCI.5255-05.2006
- Shigetomi, E., D.N. Bowser, M.V. Sofroniew, and B.S. Khakh. 2008. Two forms of astrocyte calcium excitability have distinct effects on NMDA receptor-mediated slow inward currents in pyramidal neurons. *J. Neurosci.* 28:6659–6663. doi:10.1523/JNEUROSCI.1717-08.2008
- Stout, C., and A. Charles. 2003. Modulation of intercellular calcium signaling in astrocytes by extracellular calcium and magnesium. *Glia.* 43:265–273. doi:10.1002/glia.10257
- Syková, E., and C. Nicholson. 2008. Diffusion in brain extracellular space. *Physiol. Rev.* 88:1277–1340. doi:10.1152/physrev.00027.2007
- Takahashi, T., Y. Kajikawa, and T. Tsujimoto. 1998. G-Protein-coupled modulation of presynaptic calcium currents and transmitter release by a GABAB receptor. *J. Neurosci.* 18:3138–3146.
- Turecek, R., and L.O. Trussell. 2001. Presynaptic glycine receptors enhance transmitter release at a mammalian central synapse. *Nature* 411:587–590. doi:10.1038/35079084
- von Gersdorff, H., and J.G. Borst. 2002. Short-term plasticity at the calyx of held. *Nat. Rev. Neurosci.* 3:53–64. doi:10.1038/nrn705
- Wang, L.Z., and X.Z. Zhu. 2003. Spatiotemporal relationships among D-serine, serine racemase, and D-amino acid oxidase during mouse postnatal development. *Acta Pharmacol. Sin.* 24:965–974.

Reyes-Haro et al., <http://www.jgp.org/cgi/content/full/jgp.200910354/DC1>

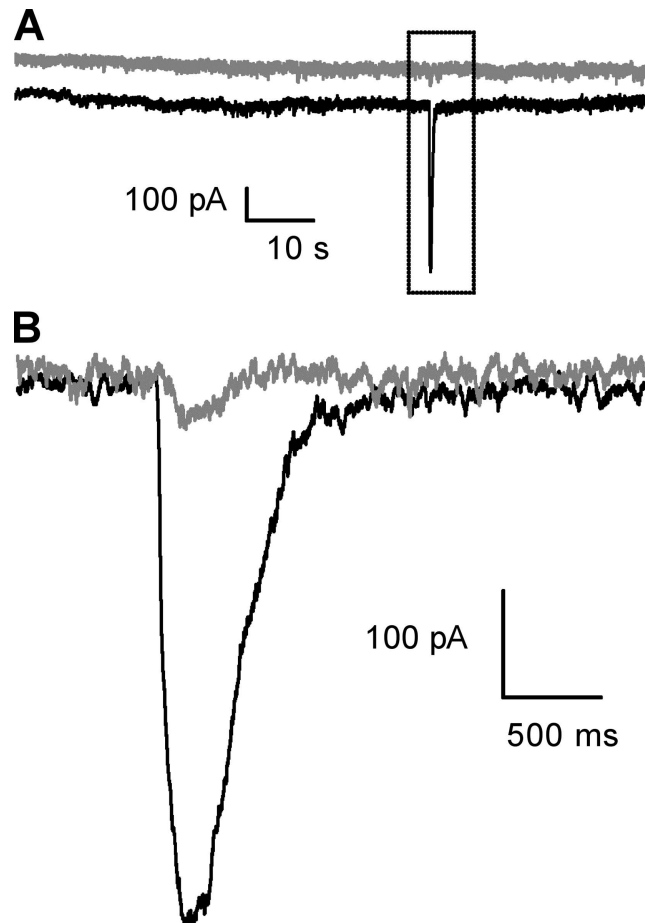


Figure S1. Representative paired recording showing synchronized nSICs. The paired recording was obtained in aCSF with low Ca^{2+} and Mg^{2+} + TTX (1 μM) + strychnine (1 μM) + gabazine (10 μM). This is one of the two paired recordings where synchrony of nSICs was observed (4 out of 50 nSICs; $n = 12$ paired recordings). (B) Synchronized nSICs are shown in higher time resolution.

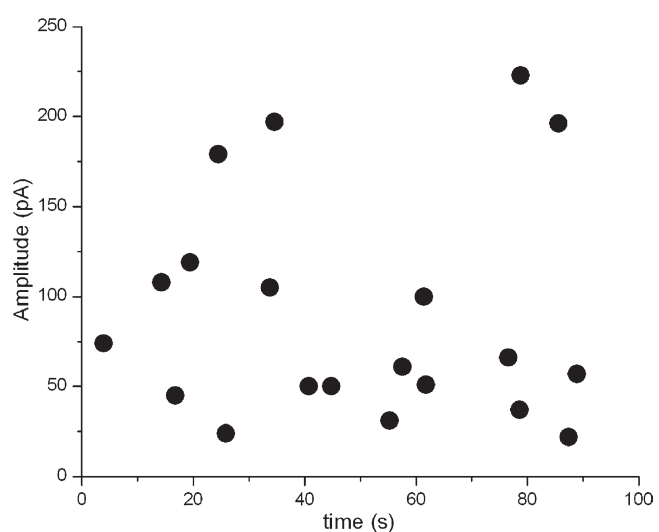


Figure S2. Raster plot showing the amplitudes and time occurrence of nSICs recorded after calcium wave evoked by electrical stimulation. The nSICs ($n = 20$ nSICs from 24 neurons) were obtained in Mg^{2+} -free aCSF + TTX (1 μM) + strychnine (1 μM) + gabazine (10 μM).

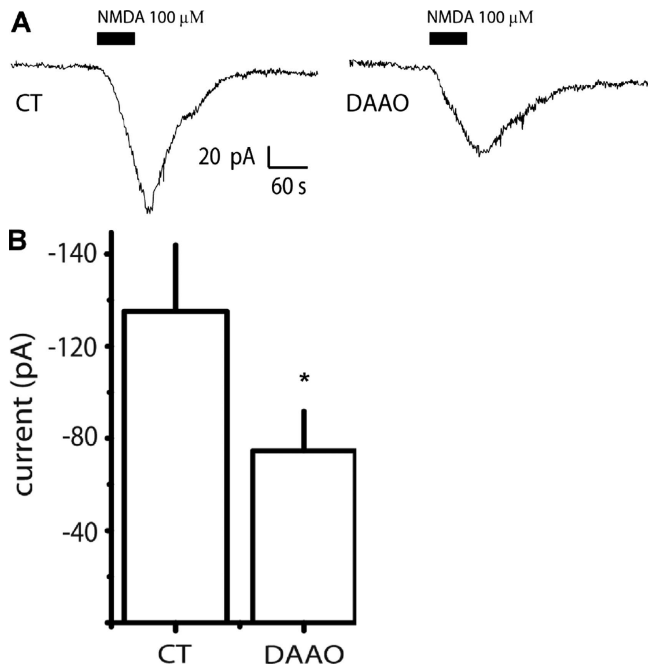
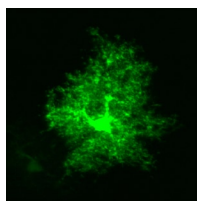


Figure S3. nSICs are reduced by degrading D-serine. (A) Representative current recordings of a PPN clamped at -70 mV. Bath application of NMDA (100 μ M) induced an inward current. The trace on the left is an example of a control current, the trace on the right after preincubation with DAAO (0.17 U/ml). (B) Summary of the effect of DAAO on NMDA currents. NMDA elicited an inward current of 135.15 ± 28.77 pA in control slices ($n = 10$). The NMDA-elicited inward current was 74.56 ± 17.22 pA ($n = 9$) when DAAO was preincubated. Data are the mean \pm SEM. Asterisk represents significant difference (*, $P = 0.04$).



Video 1. 3D reconstruction of an astrocyte in an MNTB slice, a series of 35 two-photon images were taken in steps of 1 μ m. The fluorescence is due to the expression of eGFP in the GFAP-eGFP transgenic mouse line. The reconstruction displays 51 frames at a speed of 6 frames per second, turning 360° in 7° steps. The video shows that the PPN, visible as a hollow area in the center, is completely covered by astrocytic processes and that the astrocyte soma is in close contact to the PPN. The diameter of the displayed frame is 90 μ m. Note that the astrocyte is located on the PPN like a hat on a head.

TABLE S1.
Calcium response in astrocytes increases the frequency of nSICs

	Before astrocytic calcium response	After astrocytic calcium response	n	p
Control (normal aCSF)	0.015 ± 0.010	0.058 ± 0.037	16	0.27
aCSF + TTX (1 μM)	0.011 ± 0.011	0.097 ± 0.037	16	0.036
aCSF/Mg ²⁺ free + TTX (1 μM)	0.015 ± 0.010	0.013 ± 0.050	17	0.13
aCSF/Mg ²⁺ free + TTX (1 μM) + strychnine (1 μM) + gabazine (10 μM)	0.022 ± 0.012	0.3 ± 0.1	20	0.0089
aCSF/Mg ²⁺ free + TTX (1 μM) + strychnine (1 μM) + gabazine (10 μM) + CNQX (25 μM)	0	0.179 ± 0.066	24	0.0094
aCSF/Mg ²⁺ free + TTX (1 μM) + strychnine (1 μM) + gabazine (10 μM) + CNQX (25 μM) + ifenprodil (100 μM)	0	0.006 ± 0.004	17	0.15
aCSF/Mg ²⁺ free + TTX (1 μM) + strychnine (1 μM) + gabazine (10 μM) + DAAO (0.17 U/ml)	0.04 ± 0.018	0.0096 ± 0.056	15	0.71
aCSF/Mg ²⁺ free + TTX (1 μM) + strychnine (1 μM) + gabazine (10 μM) + BAPTA (40 mM) injected in an astrocyte previously	0	0.015 ± 0.015	8	0.33

Table shows the values of experiments shown in Fig. 7 C.